International Journal of Microwave and Wireless Technologies, 2017, 9(6), 1345–1354.
doi:10.1017/S1759078717000678

RESEARCH PAPER

Waveform diversity for SAR ECCM based on random phase and code rate transition

KEE-WOONG LEE AND WOO-KYUNG LEE

In this paper, we propose an effective waveform diversity scheme that can be applicable to synthetic aperture radar (SAR) operations affected by interfering signals. A novel approach is taken to achieve fully adaptive SAR waveform diversity that generates sufficient number of orthogonal signals with modest performance trade-off. To this purpose, multiple phased-code waveforms are arbitrarily generated with mutually low cross-correlations. They exhibit a highly flexible characteristic as their code lengths are not limited and Doppler tolerance is well preserved throughout SAR imaging. Various SAR jamming simulations are carried out to demonstrate that the proposed waveform diversity has a good potential for electronic counter-countermeasures applications.

Keywords: Radar signal processing and system modeling, Radar applications

Received 31 October 2016; Revised 16 May 2017; Accepted 17 May 2017; first published online 13 June 2017

I. INTRODUCTION

In modern electronic warfare, the electronic counter-countermeasures (ECCM) capability and low probability of detection and interception (LPD/LPI) properties are constantly emphasized [1]. Recently, electronic countermeasures (ECM) against synthetic aperture radar (SAR) has been attracting attentions and various deceptive jamming techniques have been developed [2, 3]. Simple notch filters can be used against narrowband noise jammers although image qualities are sacrificed [4]. But when wideband digital radio frequency memory (DRFM) jammers are present, conventional space-domain filtering schemes cannot be practical solutions. They may not work against DRFM jamming, when the hostile signal is directly duplicated from the transmitted waveform [5]. Waveform diversity is relatively easy and simple to implement since it only requires different types of waveforms having good cross-correlation characteristics with each other. A good cross-correlation implies that the transmitted waveform is orthogonal with the DRFM signals, resulting in sufficient suppression of jamming noise [6–8].

Noise waveforms have long been attractive candidates for waveform diversity owing to their randomly orthogonal properties, efficient spectrum utilization, good ECCM capability and LPD characteristics [9]. But random noise waveforms tend to exhibit high sensitivities to Doppler shifts and extra care should be taken to maintain the phase coherence of transmit waveform in SAR application. The notion of taking random phase or chirp rate perturbations on linear frequency modulation (LFM) waveforms was introduced for SAR ECCM [6] but there still remains challenging issues in regard to Doppler sensitivity losses and acceptable orthogonal properties [10–12]. In most cases, waveform diversity adversely affects SAR image quality and becomes a complicated task of trading-off between diverse SAR image properties. In practice, there is no known analytic solution to achieve fully adaptive SAR waveform diversity that generates sufficient number of orthogonal waveforms with modest performance trade-off against direct DRFM jammers. Advanced pulse compression noise (APCN) waveform is a class of random sequence derived from LFM [13, 14] and it makes use of random perturbations on both amplitude and phase modulations to obtain noisy waveforms. However, like other noisy signals, the increased random perturbations in both amplitude and phase distributions cause considerable losses in terms of signal-to-noise ratio (SNR) and Doppler tolerance [15].

Several studies have been carried out to adopt waveform diversity techniques for wide-swath SAR missions [16, 17]. However, the previously known techniques are usually not considered for SAR ECCM due to the limited number of feasible waveforms or poor Doppler sensitivities.

In this paper, a novel waveform construction scheme is introduced to generate multiple random phase code sequences such that the performance degradation at receiver is minimized against interfering signals. For this purpose, a method of code rate triggering is implemented in conjunction with random phase perturbation to generate a group of orthogonal waveforms with flexible design parameters. To investigate the possible use for SAR ECCM, various SAR target jamming simulations are performed under possible ECM scenarios including false target and frequency shifted jamming.

Department of Electronic and Information Engineering, Korea Aerospace University, Goyang-si, Gyenggi-do, South Korea
Corresponding author:
W.-K. Lee
Email: wklee@kau.ac.kr

Finally, it is demonstrated that the proposed waveform diversity has a good potential for use in future imaging radar missions by providing flexible ECCM capability.

II. RANDOM PHASE AND CODE RATE TRANSITION TECHNIQUE

A) Waveform group generation

The phase perturbed LFM is constructed by imposing partial random perturbation on the signal phase distribution. When implementing waveform diversity of size $M(M > 1)$, we need a group of M independent phase sequences. Here, the mth waveform is implemented by imposing stochastic phase distributions $P_m(t) = \exp\{j\pi\theta_m(t)\}$ on the conventional complex LFM waveform $L(t)$ as

$$R_m(t) = L(t)P_m(t) = \exp\{j(\pi K_r t^2 + \theta_m(t))\} \quad (1)$$

where K_r is the chirp rate of LFM. Instead of using completely unpredictable noise sequences, here we adopt a strategy of using staggered partial code lengths. The code rate staggering is implemented in conjunction with random phase perturbation and hence the generated code is denoted as random phase and code rate transition (RPCR).

The code rate of stochastic phase is not fixed but continuously altered along the time sequences. Hence the waveform is constructed by a group of phase sequences having time varying partial code lengths. For the given spectrum and chirp rate, RPCR waveforms can be uniquely defined by arranging the random phase sequences of time-varying length of γ_g.

In general, the stochastic signal $P_m(t)$ of length N can be expressed as

$$P_m(t) = \sum_{n=1}^{N} \tilde{v}_{RPCR}[n] \cdot \{U(t - nt_b) - U(t - (n-1)t_b)\} \quad (2)$$

Here t_b is the bit duration, $U(t)$ is a unit step function and $\tilde{v}_{RPCR}[n]$ is the nth element of the stochastic sequence. $\tilde{v}_{RPCR}$ is comprised of G sets of subgroups. The gth subgroup is of length γ_g and has a constant phase term of $\tilde{v}_{RPCR,g} = \exp(j\theta_g)$. This can be expressed as

$$P_m(t) = \sum_{g=1}^{G} \tilde{v}_{RPCR_g} \cdot \{U(t - t_b D_g) - U(t - t_b D_{g-1})\} \quad (3)$$

where $D_g = \sum_{l=1}^{g-1} \gamma_l$. G is the total number of phase groups of $P_m(t)$. In (3), the random perturbation of RPCR or $P_m(t)$ is determined by the choice of group phase θ_g and length γ_g. Here γ_g is chosen in the interval of $[1, \ldots, \gamma_{max}]$, where γ_{max} designates the maximally allowable partial code length. θ_g is taken in $[0, 2\pi]$. γ_g can be expressed as a random variable of arbitrary discrete number distribution.

Similarly, the phase perturbation is taken by the random variable of $\theta_m = rand(0, \theta_{max})$. θ_{max} designates the depths of phase perturbation and can be set by a scaling factor ε as $\theta_{max} = 2\pi\varepsilon$. Here ε is an arbitrary number given as $0 < \varepsilon < 1$. The choice of ε and γ_{max} determines the level of random phase perturbation and the generated waveforms can be classified by these design parameters. For classification, the group waveforms of the same class are denoted by RPCR(γ, κ). Here γ and κ correspond to γ_{max} and $10 \times \varepsilon$, respectively.

Figure 1 illustrates a sample case of complex amplitude distributions and the frequency spectrum of RPCR(10,10). LFM of 60 MHz bandwidth is adopted as a basis signal to mix with a stochastic phase function in (3). There occurs a bandwidth spreading effect due to the random transition of phases. This will certainly affect overall performances and should be taken into account at the band-limited receiver.

A group of multiple RPCR waveforms can be arbitrarily constructed from the fixed pair of (γ, κ). With maximum phase perturbation of $\kappa = 10$, the phase diagrams of three distinctive RPCRs are generated for $\gamma = 1$ and $\gamma = 10$ in Fig. 2. The randomly distributed phase perturbations and time varying code lengths are easily identified in each (γ, κ) groups.

Similarly, a group of multiple RPCR waveforms can be arbitrarily constructed from the given (γ, κ) pair. While co-sharing the limited time and frequency resources, they exhibit partially noise-like characteristics. The design goal is to find a set of co-channel RPCR waveforms that maintain near orthogonal relationship with good Doppler tolerances.

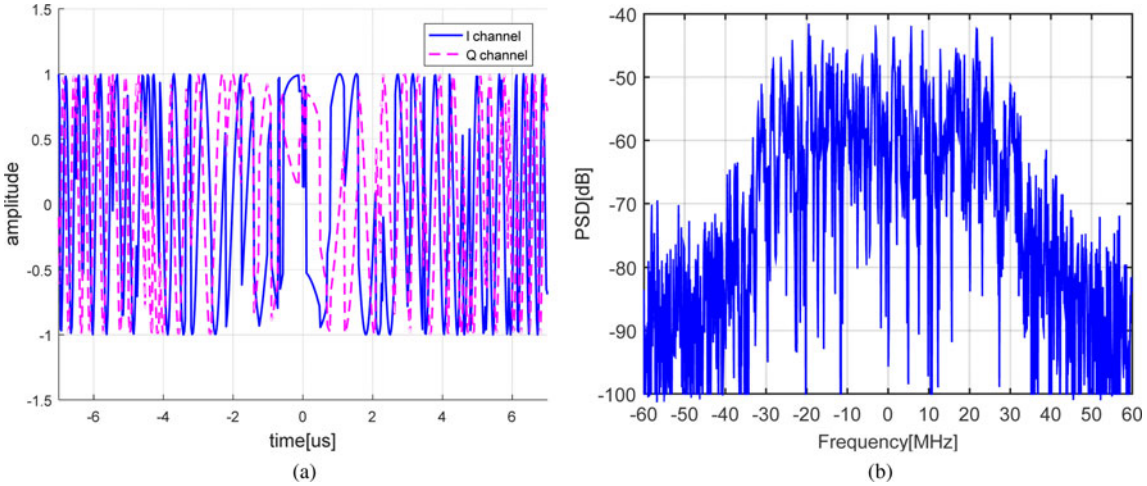

Fig. 1. RPCR waveform characteristics (a) I/Q channels in time domain and (b) power spectrum.

https://doi.org/10.1017/S1759078717000678 Published online by Cambridge University Press

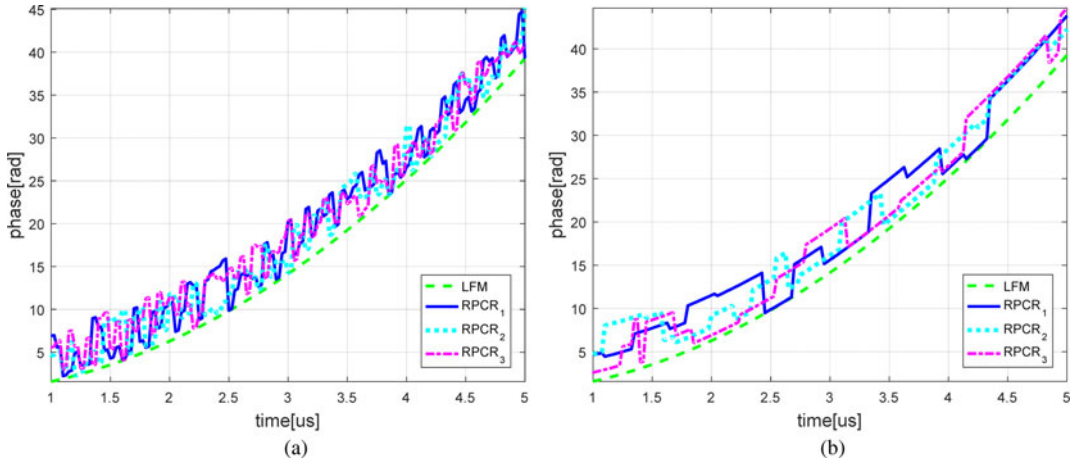

Fig. 2. Phase plots of RPCR waveform set (a) RPCR(1,10) case and (b) RPCR(10,10) case.

It turns out that a good choice of γ and κ pair helps to achieve this goal as they uniquely affect the overall performance.

B) Orthogonality and Doppler tolerance

Let the cross-correlation function (CCF) of R_i and R_j signals be given as p_{ij}. Having cross-correlation higher than autocorrelation sidelobe peak (ASP) implies that the radar detection performance is degraded due to the non-perfect orthogonality of co-existing waveforms. Multiple orthogonal waveforms may be distinguished from each other on the condition that the cross-correlation peak (CP) is lower than the minimum of ASPs [18]. This can be expressed as

$$\max\left|p_{ij}(\tau)\right| < \min[ASP(p_{ii}(\tau),\ ASP(p_{jj}(\tau)] \qquad (4)$$

In a good orthogonal code set, it is expected that there exist sufficiently large number of waveform pairs satisfying (4). To this purpose, a single RPCR waveform R_1 is generated as a reference signal. Then its cross-correlation measurements are repeatedly carried out with the newly generated RPCR waveforms R_j ($j > 1$) until (4) is met. Monte Carlo simulation is taken to select additional orthogonal waveforms that satisfy (4) with the group waveforms previously generated.

Figure 3 shows the auto-correlation function (ACF) and CCF simulation results from the thus generated pairs of RPCR(5,10) and RPCR(10,10) waveforms groups. For $\gamma = 5$ case, the CP is -21.3 dB and this is lower than ASP by 5 dB. Increasing γ to 10 slightly reduce the gap to 4.5 dB and still the good orthogonal property is preserved. In this way, multiple orthogonal waveforms can be generated for other RPCR groups. Intensive Monte Carlo simulations are taken for the different choice of γ and the average ASP and CP levels are listed in Table 1. Although the integrated sidelobe ratio (ISLR) is not a direct measure of the orthogonal property, it may affect the quality of distributed target imaging. Like APCN [13], RPCR is based on a discrete conversion of LFM and its ISLR property is comparable to typical LFM case. It can be readily shown that RPCR exhibits robust ISLR performance in proportion to ASP for all cases in Table 1.

Having higher κ is beneficial for orthogonal property as it intensifies the chaotic levels of the sequences and but at the price of extended Doppler loss. Meanwhile, the random code rate transition helps to relax phase corruption and restrain Doppler mismatching, while the noise-like phase characteristic is still maintained. In Fig. 4, the ambiguity plots of RPCR waveforms are shown as functions of range times τ and Doppler shifts υ. The time-bandwidth product BT is 800. Despite the maximum phase perturbations of $\kappa = 10$, the Doppler tolerance is steadily improved as γ is increased from 1 to 10. RPCR(1,10) has no code rate transition and exhibits poor Doppler sensitivity in Fig. 4(a). On the other hand, the benefit of using code rate transition is highlighted in Fig. 4(c), where superior Doppler tolerance is achieved with $\gamma = 10$.

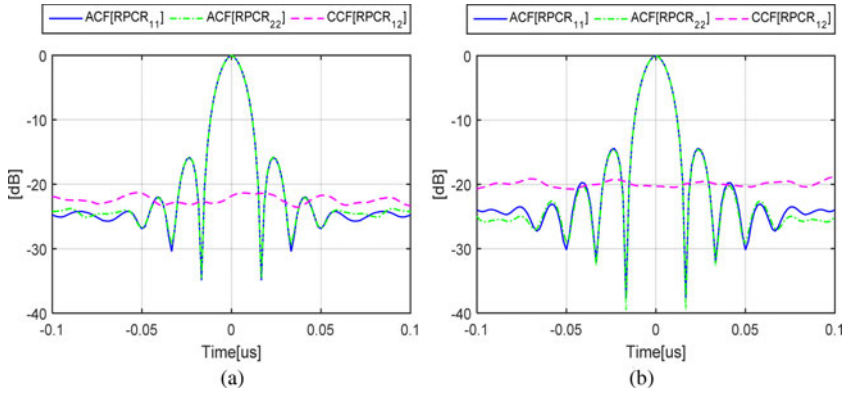

Fig. 3. ACF and CCF of RPCR (γ, κ) waveform groups (a) RPCR(5,10) and (b) RPCR(10,10).

https://doi.org/10.1017/S1759078717000678 Published online by Cambridge University Press

We have found that by selectively choosing RPCR sequences from the randomly generated groups, their Doppler losses and mutual orthogonality can be fully compromised. Hence, for the sake of good orthogonality, κ of 10 is taken for all simulations throughout this paper.

III. WAVEFORM DIVERSITY ON SAR

A) Waveform agility scheme

Waveform diversity is considered as an effective scheme for ECCM, when deceptive jamming signals are present in the received SAR signal. DRFM jammers work by detecting and regenerating the triggered pulse waveforms. However, the detection, analysis and regeneration processes take a certain period of time and hence a finite time lag should occur in most DRFM jammers [5]. Therefore, it is safe to assume that the DRFM transmit signal is not the direct duplicate of the previously received SAR pulse waveform. Under waveform diversity scheme, SAR payload varies its transmitting waveform along the azimuth slow-time in every pulse repetition interval (PRI). Meanwhile, the received signal is processed using the replica of the previously transmitted pulse. Figure 5 illustrates the SAR ECCM scenario using waveform diversity of triggering multiple codes.

Converting RPCR waveform in equation (1) into a discrete code of length N, the total set of waveforms reflected from a point target can be expressed as

$$\mathbf{s}_{\mathrm{RPCR}}[m,n]=\begin{bmatrix} \tilde{u}_{RPCR_1}[1] & \tilde{u}_{RPCR_1}[2] & \cdots & \tilde{u}_{RPCR_1}[N-1] & \tilde{u}_{RPCR_1}[N] \\ \tilde{u}_{RPCR_2}[1] & \tilde{u}_{RPCR_2}[2] & \cdots & \tilde{u}_{RPCR_2}[N-1] & \tilde{u}_{RPCR_2}[N] \\ \vdots & \vdots & \ddots & \vdots & \vdots \\ \tilde{u}_{RPCR_{M-1}}[1] & \tilde{u}_{RPCR_{M-1}}[2] & \cdots & \tilde{u}_{RPCR_{M-1}}[N-1] & \tilde{u}_{RPCR_{M-1}}[N] \\ \tilde{u}_{RPCR_M}[1] & \tilde{u}_{RPCR_M}[2] & \cdots & \tilde{u}_{RPCR_M}[N-1] & \tilde{u}_{RPCR_M}[N] \end{bmatrix} \tag{5}$$

The size of the orthogonal waveform set should be increased in proportion to the PRI and antenna aperture length and given as $M = T_a \times PRF$. Here T_a is aperture time and PRF is the pulse repetition frequency. Mutually orthogonal RPCR waveforms can be arbitrarily generated from the group class of (γ, κ). As their code lengths are not limited, the size of $\mathbf{s}_{\mathrm{RPCR}}$ is freely extended to suit for the given SAR geometry.

In pulsed spaceborne SAR system, 'stop and go approximation' is valid [19] and the mth echo signal is processed by the mth receiver of the corresponding matched filter matrix. This can be expressed by the discrete convolution of

$$\mathbf{p}_{SS^*}=\sum_{k=-N}^{k=N}\mathbf{s}_{\mathrm{RPCR}}[m,n]\mathbf{s}^{\mathrm{H}}_{\mathrm{RPCR}}[m,n-k] = \begin{bmatrix} p_{11}[k] & p_{12}[k] & \cdots & p_{1(M-1)}[k] & p_{1M}[k] \\ p_{21}[k] & p_{22}[k] & \cdots & p_{2(M-1)}[k] & p_{2M}[k] \\ \vdots & \vdots & \ddots & \vdots & \vdots \\ p_{(M-1)1}[k] & p_{(M-1)2}[k] & \cdots & p_{(M-1)(M-1)}[k] & p_{(M-1)M}[k] \\ p_{M1}[k] & p_{M2}[k] & \cdots & p_{M(M-1)}[k] & p_{MM}[k] \end{bmatrix} \tag{6}$$

The diagonal elements of (6) are ACFs and the others designate CCF. The orthogonal waveform selection is performed through an iteration process such that all the ACF and CCF elements satisfy (4). Here, SAR range Doppler algorithm (RDA) [19] is taken and after azimuth compression, the SAR point target response (PTR) is obtained as

$$s_{\mathrm{AZC}}(\tau,\eta)=W_a(\eta)\,p_{mm}\left(\tau-\frac{2R(\eta)}{c}\right)\times p_a(\eta) \times \exp\left(-\frac{j4\pi f_o R_o}{c}\right)\exp(j2\pi f_{\eta_c}\eta) \tag{7}$$

$W_a(\eta)$ is the normalized amplitude, while f_o and f_{η_c} represents the center frequency and Doppler centroid of the incoming signal. p_{mm} designates the range compression response and corresponds to diagonal element of (6). $p_a(\eta)$ is the azimuth compression response and usually represented as a sinc function.

Figure 6 illustrates SAR PTRs obtained by using RPCR waveforms of three different classes. Target responses are comparable to LFM case but with slight losses in ISLR and PSLR (peak sidelobe ratio). It appears that having low γ is advantageous in terms of sidelobe level but it is simply attributed to bandwidth extension effect and will be compensated for after finite bandwidth filtering. It will be discussed in next section. Nevertheless, given the superior Doppler tolerance, the performance degradation may be acceptable for all cases.

B) Bandlimit constraint

Unlike LFM, the power spectrum of the phase-coded signal spreads out indefinitely and SNR loss occurs due to the imperfect matching at the receiver. The matched filter simulations are performed with the bandlimit constraint considered and the results are shown in Fig. 7. As expected, RPCR(1,10) suffers from -4 dB loss and hence the merit of having chaotic sequence is impaired. This is attributed to the extended bandwidth spreading effect by the random phase perturbation.

On the other hand, the SNR loss is reduced to -1.3 dB as γ is increased to 5. It is further improved as -0.8 dB for $\gamma = 10$

https://doi.org/10.1017/S1759078717000678 Published online by Cambridge University Press

Table 1. ASP and CP levels of RPCR groups.

Waveform	ASP [dB]	CP [dB]
RPCR(1,10)	−27.91	−28.22
RPCR(5,10)	−16.09	−21.30
RPCR(10,10)	−14.57	−18.92
RPCR(20,10)	−13.91	−15.41

and −0.3 dB for $\gamma = 20$ and becomes comparable to the original LFM case. This can be explained by the smoothing effect of higher code rate transition that gives rise to the reduction of the abrupt phase changes.

Waveform design is a process of performance trade-off for the specific radar application. In this paper, the maximum depth of phase perturbation ($\kappa = 10$) is applied for RPCR waveform generation to obtain superior orthogonality. Then, the code rate factor γ over 5 is taken in order to minimize the SNR loss and maintain orthogonality and Doppler tolerance. Figure 8 shows the simulated SAR PTR cases using RPCR waveform diversity. Two waveforms are selected from RPCR(5,10) group and their PTRs are analyzed with and without bandwidth limiting. They exhibit relatively good performances comparable to conventional LFM cases [16], while their orthogonality is verified through the co-channel PTRs.

IV. SAR ECCM BASED ON WAVEFORM DIVERSITY

A) SAR deceptive jamming

Since the DRFM jamming signals are coherent with the original SAR signal, false targets can be intentionally generated in the processed SAR images. This is known as false target jamming (FTJ) and regarded as a potential threat to the military radar mission [20]. Randomly or stepped frequency shifting jamming (RFSJ or SFSJ) can cause barrage effects and mask a portion of SAR image [21, 22]. A demodulated FSJ (frequency shifting jamming) signal can be expressed in two-dimensional functions as

$$\begin{aligned} s_{jbb}(\tau, \eta) = {} & \sqrt{P_j(\eta)} w_r\left[\tau - \tau_{d_{tgt}}(\eta)\right] w_a[\eta - \eta_{jc}] \\ & \times \exp\left\{-\frac{j4\pi f_o \tau_{d_{tgt}}(\eta)}{2}\right\} s[\tau - \tau_{d_{tgt}}(\eta)] \\ & \times \exp[j2\pi f_{d_{fast}}\{\tau - \tau_{d_{tgt}}(\eta)\}] \exp\{j2\pi f_{dslow}(\eta)\} \end{aligned} \tag{8}$$

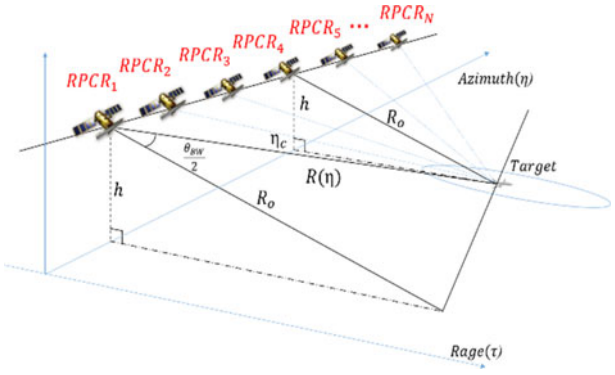

Fig. 5. SAR target imaging based on multiple code triggering scheme.

τ is the fast time in range, η is the slow time in azimuth and $R_j(\eta)$ is the range between the SAR sensor and jammer. For convenience, the jamming signal power is given as $P_j(\eta)$, while w_r and w_a are range and azimuth antenna patterns. The received signal in DRFM is duplicated, modified and re-transmitted with a time delay $\tau_{d_{tgt}}(\eta)$ to produce false targets. $f_{d_{fast}}$ is derived from the random frequency perturbation of the RFSJ signal and contributes to producing arbitrary ghost patterns in SAR images. In SFSJ case, linear frequency perturbation is applied in f_{dslow} leading to the barrage effects.

The use of conventional interference mitigating process, i.e. notch or LMS (Least Mean Square) filter is not practical in suppressing these deceptive jamming signal, as the interfering signal is distributed over wide bandwidth and overlapped with the target signal.

B) SAR ECCM technique against deceptive jamming

Figure 9 illustrates the SAR ECCM scenario using waveform diversity. In this scenario, the transmitted SAR signal is arbitrarily selected from a group of programmed RPCR waveforms. The waveform sequence of the SAR system and DRFM jammer are expressed as

$$w_{RPCR\eta}(\tau), \quad \eta = 1, 2, \ldots M \tag{9}$$

$$w_{JAM\eta}(\tau) = w_{RPCR\eta-l}(\tau), \quad \kappa > 1 \tag{10}$$

M is the number of orthogonal RPCR waveforms and l is the sequence lag of the jamming signal. For ECCM

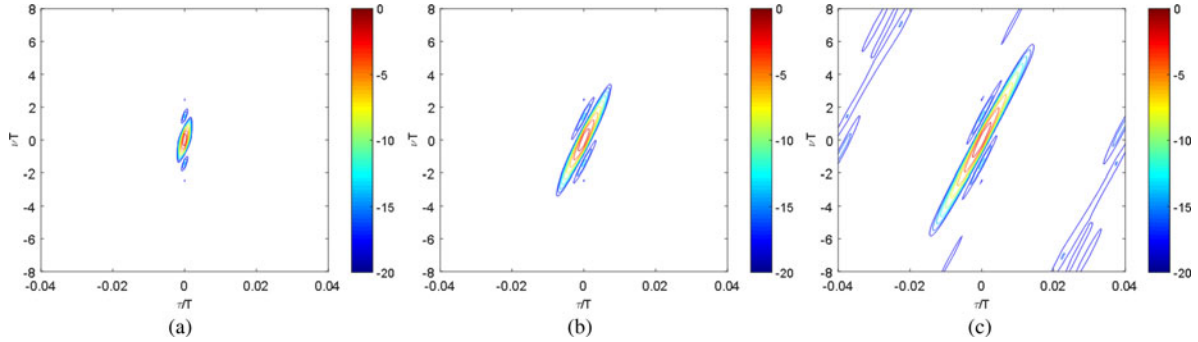

Fig. 4. Ambiguity function plots [dB] (a) RPCR(1,10), (b) RPCR(5,10), and (c) RPCR(10,10).

https://doi.org/10.1017/S1759078717000678 Published online by Cambridge University Press

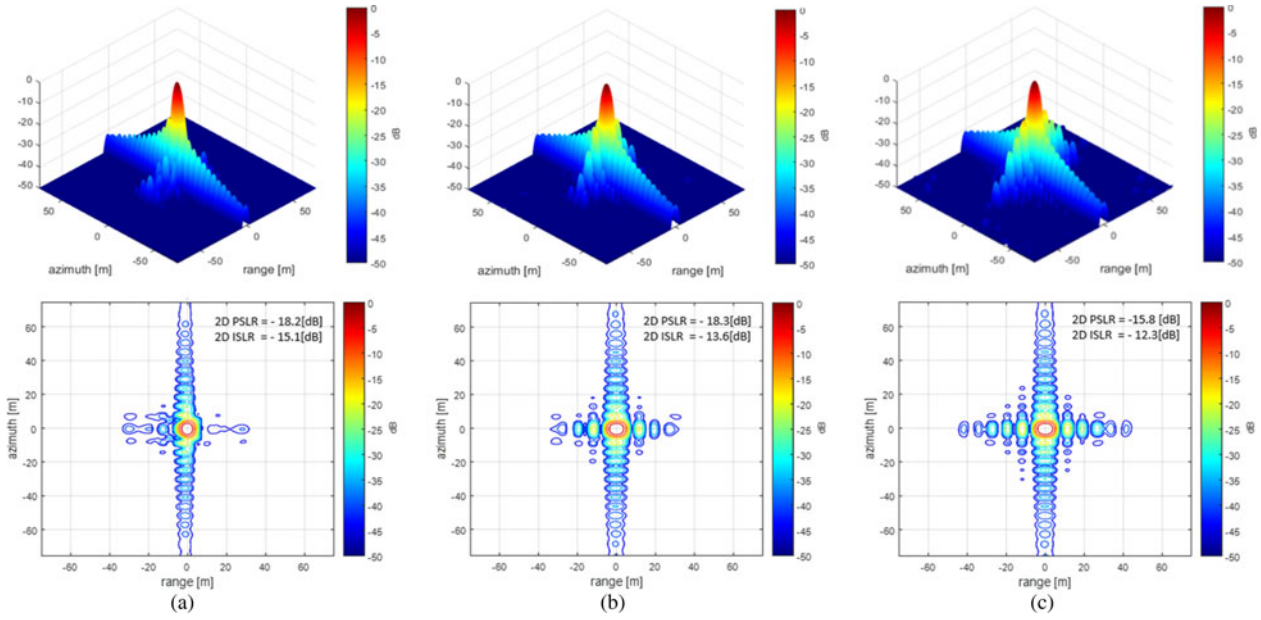

Fig. 6. SAR impulse responses with (a) RPCR(1,10), (b) RPCR(5,10), and (c) RPCR(10,10).

implementation, the signal transmitted by a DRFM repeat jammer should be sufficiently orthogonal to the SAR signal received simultaneously at current azimuth slow-time.

The total received signal can be expressed by

$$s_{bb}(\tau,\eta) = s_{r_{bb}}(\tau,\eta)_{RPCR_m} + s_{jbb}(\tau,\eta)_{RPCR_{m-l}} + n(\tau,\eta) \quad (11)$$

Here $s_{r_{bb}}$ is the original SAR signal and correspond to the mth RPCR pulse sequence shown in (7). $s_{jbb}(\tau,\eta)_{RPCR_{m-l}}$ is a duplicated DRFM waveform. It is a time-lagged pulse delayed by l within the transmit waveform trains and should be sufficiently orthogonal to the current SAR signal in the air or $s_{r_{bb}}(\tau,\eta)_{RPCR_m}$. The $n(\tau,\eta)$ represents additional clutter noise. As in (11), RDA SAR processing of (11) results in

$$s_{AZC}|_{ECCM}(\tau,\eta) = \sqrt{P_s(\eta)}\, p_{mm}\left(\tau - \frac{2R_o}{c}\right) p_a(\eta)\exp\{j\theta_t(\eta)\} + \sqrt{P_J(\eta)}\, p_{m(m-l)}\left(\tau - \frac{2R_{j_o}}{c}\right) p_a(\eta)\exp\{j\theta_J(\eta)\} \quad (12)$$

$\theta_t(\eta)$ is the original azimuth phase, $\theta_J(\eta)$ is the phase displacement by the jamming signal. P_S is derived from the original signal level of $s_{r_{bb}}$ and calculated from p_{mm} in (6). P_J represents the unwanted jamming effect caused by s_{jbb} and should be minimized. This can be implemented by the cross-correlation operation between mth and $(m-l)th$ RPCR waveforms, which is equivalent to $p_{m(m-l)}$ in (6). DRFM jamming signals are mixed with the original SAR reflections but will be weakened in the range compression process and hence suppressed in proportion to $|p_{m(m-l)}|$ at the final SAR image.

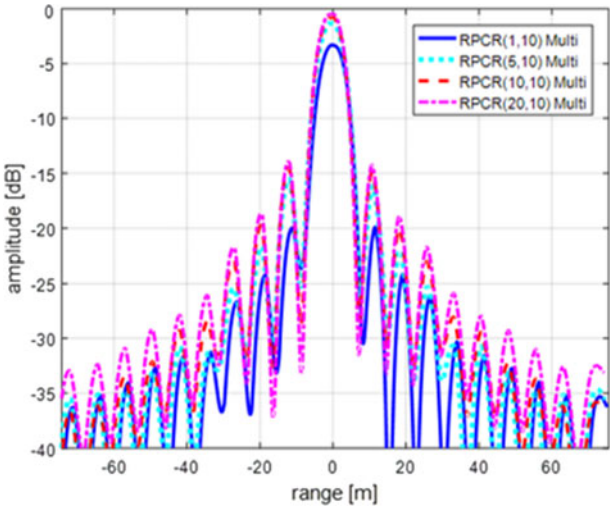

Fig. 7. Range profiles for RPCR waveforms at bandlimited receiver.

C) SAR ECM and ECCM simulation

Based on the point target analysis in previous sections, SAR simulation are carried out to assess the proposed ECCM scheme under various ECM scenarios. In simulation, C-band spaceborne SAR parameters [19] are employed and four point targets (2 by 2 position) are assumed on the ground. Figure 10 shows the geometry of the point targets and DRFM jammer. The SAR sensor moves with velocity of 6.8 km/s and its minimum slant range to the reference target is given as 683 km. The employed SAR signal has a time-bandwidth product of 800 and is transmitted with PRF of 1.61 kHz. It is assumed that the DRFM jammer is located at a distance of 350 m from the closest target.

To assess the effects of ECM and ECCM, the effective radiated power (ERP) density of the jamming signal is calculated in the processed SAR image [20]. In (13), P_S and P_J

https://doi.org/10.1017/S1759078717000678 Published online by Cambridge University Press

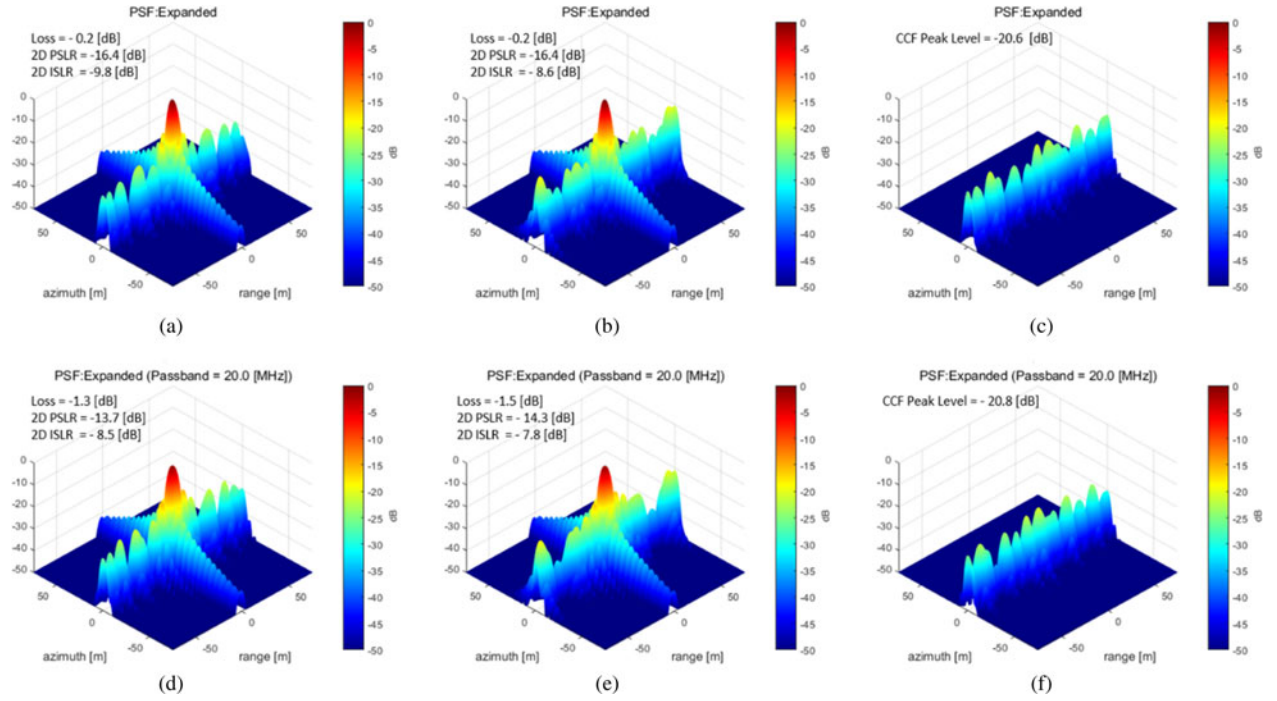

Fig. 8. SAR PTRs of two $RPCR_1$ and $RPCR_2$ from RPCR(5,10) group: before (top) and after (bottom) bandlimiting (a),(d) $RPCR_{11}$ (b),(e) $RPCR_{22}$ (c),(f): cross-channel responses.

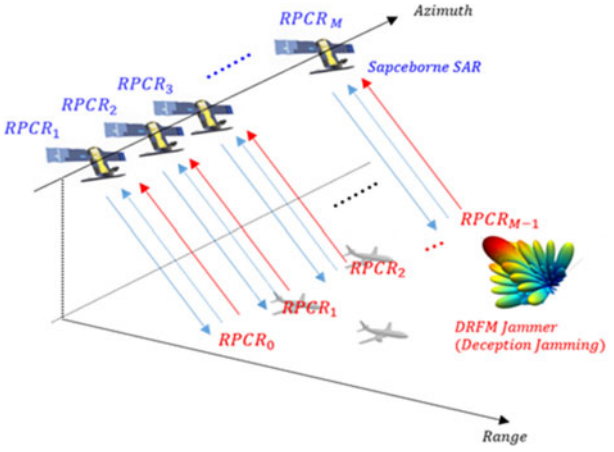

Fig. 9. Waveform diversity scenario for SAR ECCM.

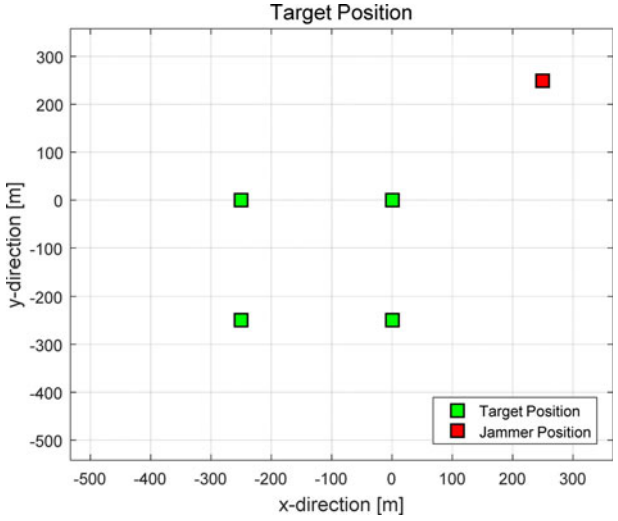

Fig. 10. Geometry of point targets and jammer.

correspond to ERPs of SAR and jamming signals. Then, their relative ratio $ERP_{S/J}$ is taken as a jamming effect measure in (14). The jamming effects appear in unique manners for different ECM scenarios. For a fair comparison, different $ERP_{S/J}$ levels of 99.33, 74.33 and 84.33 dB are applied for false target, random frequency shifting and SFSJ, respectively.

$$P_s = \frac{P_{ST} G_T G_R \lambda^2 G}{(4\pi)^3 R_s^4 L_s}, \quad P_J = \frac{P_{JT} G_J G_R \lambda^2 G}{(4\pi R_J)^2 L_J} \tag{13}$$

$$ERP_{S/J} = \frac{P_{ST} R_J^2}{P_{JT} 4\pi R_S^4} \approx \frac{P_{ST}}{P_{JT} 4\pi R_S^2}, R_s \approx R_J \tag{14}$$

P_{ST}, P_{JT}: peak transmit power of the SAR/Jammer, G_T, G_J: antenna gain of the SAR/Jammer, G_R: receiver antenna gain of the SAR/Jammer, R_J, R_S: range between target and SAR/Jammer, L_s, L_J: total system losses of SAR/Jammer.

ECM simulations are performed with LFM, while RPCR waveform diversity is employed for ECCM tests and the results are shown in Fig. 11. In Fig. 11(a), when FTJ is applied, a false target response shows up near the true targets. In Fig. 11(b), RFSJ causes masking effect on the target scene. SFSJ produces a barrage effect casting a distributed shadow in Fig. 11(c). In this case, the coherent jamming effect is focused on a narrow area and consequently, the true targets are completely obscured and cannot be identified.

https://doi.org/10.1017/S1759078717000678 Published online by Cambridge University Press

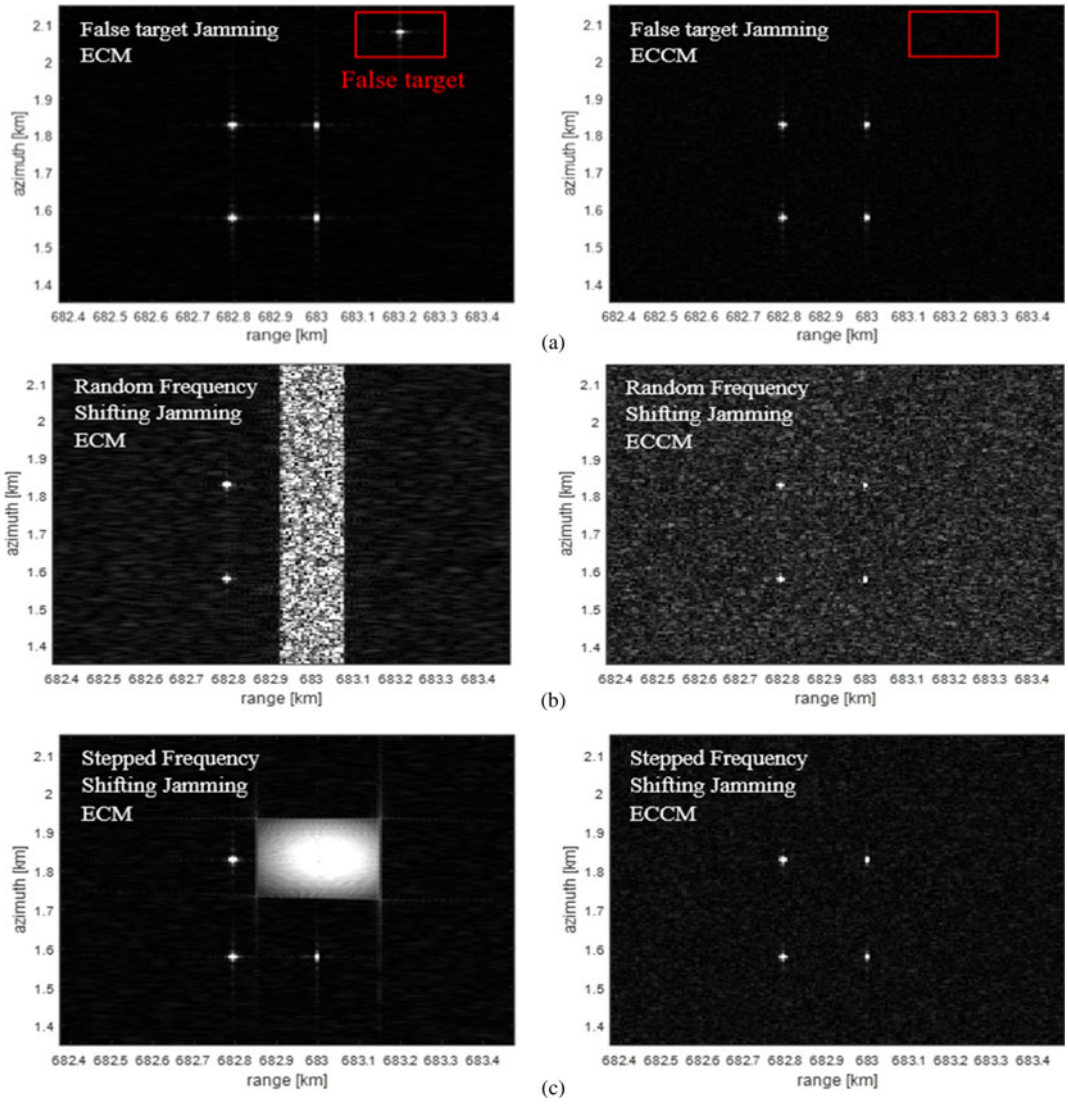

Fig. 11. Deceptive jamming effects and SAR ECCM simulations for RPCR(5,10) (a) FTJ, (b) RFSJ, and (c) SFSJ.

Then, the proposed ECCM scheme is applied and the right part images of Fig. 11 are produced through RPCR(5,10) waveform diversity. Although the image qualities are slightly impeded, it is seen that the jamming effect is effectively removed thus improving the target detection capability. For further verification J/C (jamming to clutter ratio) and S/(J + C) (signal to jamming and clutter ratio) are taken to measure the image qualities and summarized in Table 2.

Table 2. Quality analysis of RPCR waveform diversity for SAR ECCM.

Waveform	FTJ (J/C) [dB]	RFSJ (S/J + C) [dB]	SFSJ (S/J + C) [dB]
Linear-FM	48.45	17.08	11.77
RPCR(5,10)	7.32	25.04	34.77
RPCR(10,10)	7.63	23.06	32.40
RPCR(20,10)	7.63	20.94	30.25

FM, frequency modulation.

When LFM is adopted, the image qualities are significantly degraded with 48.45 dB of J/C, 17.8 and 11.77 dB of S/J + C. But when LFM is substituted with RPCR and the multiple waveform diversity scheme is employed, J/C is reduced down to 7 dB and S/(J + C) is increased over 30 dB. These results validate the superior performance of RPCR waveform diversity against DRFM jamming effects.

Figure 12 shows SAR simulation results when three airplane targets are located near DRFM jammer. In Fig. 12(a), a single RPCR(5,10) only is employed and the barrage effect intrudes target response above threshold level. On the other hand, deceptive jamming effect is practically removed in Fig. 12(b) after multiple waveform diversity scheme is applied.

Finally, SAR raw data simulations are carried out in Fig. 13. Figure 13(a) shows SAR images distorted and masked by the barrage ECM effect when conventional LFM is employed. On the other hand, Fig. 13(b) illustrates that the corrupted SAR image is restored through RPCR waveform diversity scheme. All the simulation results verify that the proposed multiple waveform diversity is an effective technique to mitigate the

https://doi.org/10.1017/S1759078717000678 Published online by Cambridge University Press

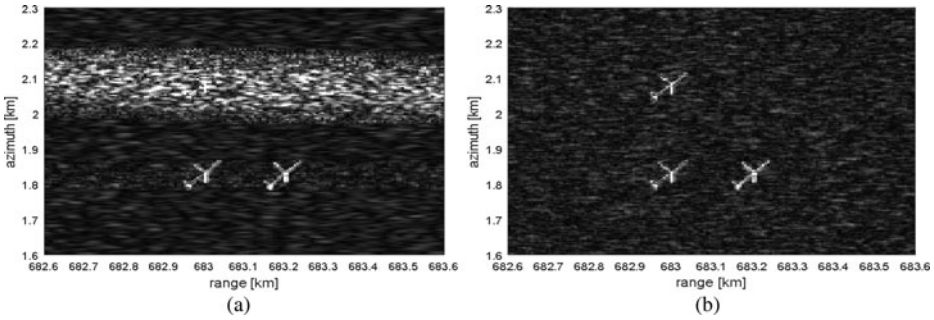

Fig. 12. SAR ECCM against deceptive jamming (a) mono code scheme and (b) waveform diversity scheme.

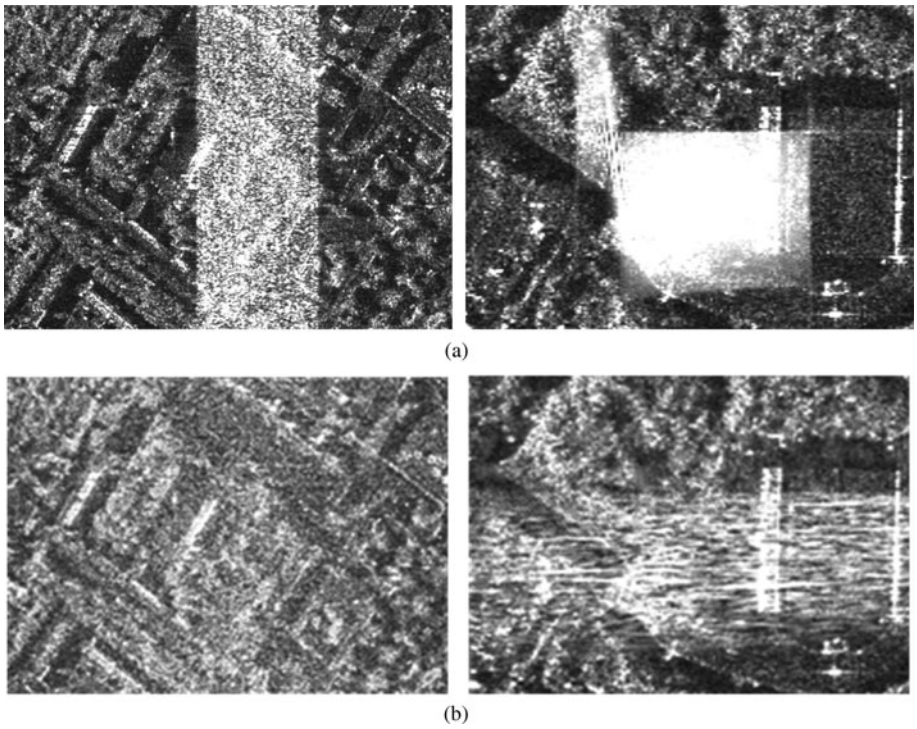

Fig. 13. SAR raw data simulations under RFSJ and SFSJ barrage effect scenarios (a) LFM and (b) RPCR waveform diversity.

DRFM jamming effects and prevent the loss of critical information.

V. CONCLUSION

For the successful application of waveform diversity for SAR imaging, multiple number of orthogonal codes are required with a good performance compromise between Doppler tolerance, bandwidth limiting and cross-correlation levels. The proposed RPCR waveform diversity is distinguished with its high flexibility. It can be conveniently applied to provide a good performance trade-off and preserve the SAR image quality simultaneously. To investigate the possible use for SAR ECCM purpose, various SAR target jamming scenarios are considered and the superior performance is verified. Through intensive simulations, it is fully demonstrated the proposed scheme maintain robust performances against ECM attacks of false target and frequency shifted jamming. It is claimed that the proposed waveform diversity has a promising potential for use in future imaging radar missions by providing robust ECCM capability.

ACKNOWLEDGEMENT

This work was supported by 2016 Korea Aerospace University faculty research grant.

REFERENCES

[1] Dmitriy, S.G.; Ram, M.N.: ECCM capabilities of an ultrawideband bandlimited random noise imaging radar. IEEE Trans. Aerosp. Electron. Syst., **38** (4) (2002), 1243–1255.

[2] Zhao, B.; Zhou, F.; Tao, M.; Zhang, Z.; Bao, Z.: Improved method for synthetic aperture radar scattered wave deception jamming. IET Radar Sonar Nav., **8** (8) (2014), 971–976.

https://doi.org/10.1017/S1759078717000678 Published online by Cambridge University Press

[3] Zhou, F.; Zhao, B.; Tao, M.; Bai, X.; Chen, B.; Sun, G.: A large scene deceptive jamming method for space-borne SAR. IEEE Trans. Geosci. Remote Sens., **51** (8) (2013), 4486–4495.

[4] Luc, K.; Jansen, R.W.; Kersten, P.R.; Fiedler, R.L.: A novel method for removal of emitter noise in SAR images. IEEE Trans. Geosci. Remote Sens. Lett., **4** (2) (2007), 265–268.

[5] Jabaran, A.: Orthogonal block coded ECCM schemes against repeat radar jammers. IEEE Trans. Aerosp. Electron. Syst., **45** (3) (2009), 1218–1226.

[6] Soumekh, M.: SAR-ECCM using phase-perturbed LFM chirp signals and DRFM repeat jammer penalization. IEEE Trans. Aerosp. Electron. Syst., **42** (1) (2006), 191–205.

[7] Lu, G.; Lia, S.N.; Luo, S.C.; Tang, B.: Cancellation of complicated DRFM range false targets via temporal pulse diversity. Prog. Electromagn. Res. C, **16** (2010), 69–84.

[8] Schuerger, J.; Garmatyuk, D.: Multifrequency OFDM SAR in presence of deception jamming. EURASIP J. Adv. Signal Proc., **2010** (1) (2010), 451851.

[9] Kulpa, K.; Lukin, K.; Miceli, W.; Thayaparan, T.: Signal processing in noise radar technology [Editoral]. IET Radar Sonar Nav., **2** (2008), 229–232.

[10] Wang, W.-Q.: MIMO SAR chirp waveform diversity design with random matrix modulation. IEEE Trans. Geosci. Remote Sens., **53** (3) (2015), 1615–1625.

[11] Farhan, A.Q.; Adly, T.F.: Doppler tolerant and detection capable polyphase code set. IEEE Trans. Aerosp. Electron. Syst., **51** (2) (2015), 1123–1135.

[12] Uttam, K.M., Mark, R.B.; Muralidhar, R.: A novel approach for designing diversity radar waveform orthogonal on both transmit and receive, in IEEE Radar Conf., 2013, 1–6.

[13] Govoni, M.A.; Elwell, R.A.: Radar spectrum spreading using advanced pulse compression noise (APCN), in IEEE Radar Conf., 2014, 1471–1475.

[14] Govoni, M.A.; Elwell, R.A.: SAR image quality using advanced pulse compression noise (APCN), in SPIE Defense+ Security, International Society for Optics and Photonics, 2014, 90770K–90770K.

[15] Govoni, M.A.; Li, H.: Range-Doppler resolution of the linear-FM noise radar waveform. IEEE Trans. Aerosp. Electron. Syst., **49** (1) (2013), 658–663.

[16] Kreiger, G., Gebert, N.; Moreira, A.: Multidimensional waveform encoding: a new digital beamforming technique for synthetic aperture radar remote sensing. IEEE Trans. Geosci. Remote Sens., **46** (1) (2008), 31–46.

[17] Wang, W.-Q.: MIMO SAR using chirp diverse waveform for wide-swath remote sensing. IEEE Trans. Aerosp. Electron. Syst., **48** (4) (2012), 3171–3185.

[18] Deng, H.: Polyphase code design for orthogonal netted radar systems. IEEE Trans. Signal Proc., **52** (11) (2004), 3126–3135.

[19] Ian, G.C.; Frank, H.W.: Digital Processing of Synthetic Aperture Radar Data, Artech House, Boston, 2005.

[20] Rebecca, S.H.; Mervin, C.B.: A study on SAR noise jamming and false target insertion, in IEEE SOUTHEASTCON, 2014, 1–8.

[21] Hong-xu, H.; Zhi-tao, H.; Yi-yu, Z.: Jamming research to SAR based on frequency characteristic, in International Conference on Signal Processing Systems (ICSPS), 2010, 114–147.

[22] Zhang, H.; Tang, Y.; Wu, G.; Sun, L.: SAR deceptive jamming signal simulation, in Asian and pacific Conference on Synthetic Aperture Radar (APSAR), 2007, 5–9.

Kee-Woong, Lee received the B.S. degree in Avionics and Electrical Engineering from Korea Aerospace University, Goyang, Korea in 2015. He is currently working toward the M.S degree in Electronic and Information Engineering at Korea Aerospace University. His current research interests include synthetic aperture radar (SAR) signal processing, radar signal processing and waveform design as well as microwave remote sensing.

Woo-Kyung, Lee received the B.S. and M.S. degree in Electrical Engineering in Korea Advanced Institute of Science and Technology(KAIST) in 1990 and 1994, respectively; and Ph.D. degree in Electrical Engineering from Univeristy College London(UCL) in 2000. From 1999 to 2003, he was a reseach professor with Satellite Technology Research Center, Daejeon, Korea. He is currently an associate professor with the school of electronic and information engineering, Korea Aerospace University, Goyang, Korea. His research interests include radars, satellite systems, synthetic aperture radar (SAR) and waveform design as well as microwave remote sensing.

https://doi.org/10.1017/S1759078717000678 Published online by Cambridge University Press